Engineering Science & Technology
https://ojs.wiserpub.com/index.php/EST/

UNIVERSAL WISER PUBLISHER

Research Article

Effect of Radiation on Casson Hybrid Nano-fluid Flow over an Inclined Surface Using Blasius Rayleigh-Stokes Variable: Application in Solar Aircraft

Olayinka Akeem Oladapo[1], Olusegun Adebayo Ajala[1], Akintayo Oladimeji Akindele[1*], Adebowale Martins Obalalu[2]

[1]Department of Pure and Applied Mathematics, Ladoke Akintola University of Technology, Ogbomoso, Oyo State, Nigeria
[2]Department of physics, Augustine University, Ilara-epe, Lagos State, Nigeria
Email: aoakindele21@lautech.edu.ng

Received: 5 December 2023; **Revised:** 26 January 2024; **Accepted:** 22 February 2024

Abstract: Solar energy is the most important heat source from the sun, with photovoltaic cells, solar power plates, photovoltaic lights, and solar water pumping being widely used. This study looks at solar energy analysis and a method for increasing the efficacy of solar aircraft by combining solar and nano-technological energy. To enrich the research on solar aircraft wings, the study is based on the investigation of heat transfer by employing a hybrid nano-fluid past inside the Parabolic Trough Solar Collector (PTSC). The thermal source is referred to as the solar radiative flow. The heat transfer efficiency of the wings was validated for different qualities such as porous medium, viscous dissipation, play heating, and thermal energy flow. The modelled energy and momentum equations were controlled by utilizing the Galerkin-Weighted Residual Method (GWRM). This study used two types of nano-solid particles, copper (Cu) and zirconium dioxide (ZrO_2), in Ethylene Glycol (EG) as the standard fluid. Various control parameters for velocity, temperature profiles, friction factor, and Nusselt number were explained and shown in figures and tables. Also, analyses reveal that the thermal profile reduces with an increase in variable thermal conductivity parameters. This study will be of considerable economic value to marine engineers, mechanical engineers, physicists, chemical engineers, and others since its application will help them improve their operations. The findings revealed that the magnetic term is positively impacted by the Cu-ZrO_2/EG hybrid nanofluid's thermal distribution.

***Keywords*:** Casson fluid, Blasius Rayleigh-Stokes variable, magnetic, variable viscosity, Galerkin-weighted residual method

Nomenclature

μ_{hnf}	Mixture nanofluid functional viscidness
Nd	Thermal radiation parameter
Γ_q	Magnetic inclination parameter
h_f	Heat transfer coefficient
B_0	Magnetic field strength

DOI: https://doi.org/10.37256/est.5220244046

Nu_x	Local nusselt number
μ	Dynamic viscosity of the fluid
u, v	Velocity components in x and y
hnf	Hybrid nanofluid
f	Base fluid
k	Thermal conductivity
x, y	Dimensional space coordinates
σ_{hnf}	Electrical conductivity of the hybrid nanofluid
Ec	Eckert number
$(\rho C_p)_{hnf}$	Specific heat capacity of the hybrid nanofluid
Pr	Prandtl number
ρ_{hnf}	The density of the hybrid nanofluid
β	Casson parameter
μ_{nf}	Dynamical viscidness of the nanofluid
$(KP)_0$	Permeability coefficient
σ_{nf}	Electrical conductivity of the nanofluid
M	Magnetic parameter
ρ_{nf}	The density of the nanofluid
t	Time
$(\rho Cp)_{nf}$	Specific heat capacity of the nanofluid
T	Temperature of fluid
q_w	Heat flux
ϕ	The volume fraction of nanoparticles
k^*	Absorption coefficient
α	Ablation parameter/leading edge accretion
θ	Dimensionless temperature
η	Independent similarity variable

1. Introduction

In recent years, due to the depletion of fossil fuels, and the rising expense of traditional types of energy, such as electricity, solar Energy has gained considerable attention.

The burning of fossil fuels discharges carbon into the atmosphere, whereas producing renewable energy does not contribute to emitting greenhouse gases. Solar energy is among the most reliable, affordable, and ecologically beneficial kinds of energy available on Earth [1]. Solar energy can create four megawatts of power, approximately three hundred times more than the amount of electricity now utilized on a global basis [2]. New research estimates that worldwide Carbon emissions will be cut by 75% by 2050 compared to 1985 levels [3]. According to the study undertaken by the United States Department of Energy, the annual energy needed for the whole globe could be fulfilled by direct sunlight hitting the earth's surface for only one and a half hours [3]. This discovery was made public in a United States report. As a natural alternative energy source, solar energy will play an important role. Solar systems, on the other hand, produce heat energy used in household appliances. As a result, the major concern is how to capture solar energy.

The two basic ways for turning sunshine into electricity are photovoltaic (PV) systems and concentrated solar energy (CSE). Some of the most important applications that may be accomplished using PV systems are as follows: Solar power plants, satellite power generators in spacecraft, and remote area power supply (RAPS), which comprises generators, lamps, and radio transmitters, are all examples of renewable energy sources [1]. A photovoltaic device's main component is an example of a semiconductor, which is a type of material that can carry many electrons. The ability of the solar cell surface to receive sunlight causes electrons to vibrate, resulting in the generation of electrical current as it passes through the semiconductor device. Concentrated solar power is a technique that harnesses concentrated solar energy for use in agriculture (concentrating solar power plant) [1]. The following is the method by which concentrated

solar power transforms energy: Massive mirrors or lenses are used to focus the sun's light, which next changes to generate heat (thermal energy), and finally, electricity is produced after the heat has passed through an electrical power generator [2]. Due to the environment, desert locales in the United States, such as California and Arizona, are ideal for creating bigger facilities using concentrated solar power. It is superior to other sources of energy since it is renewable and does not contribute to the release of harmful pollutants. In conclusion, solar energy is preferred over other types of energy since it is a renewable resource and does not emit harmful pollutants, unlike fossil fuels. Figure 1 depicts the Schematic diagram of the parabolic trough solar collector [4].

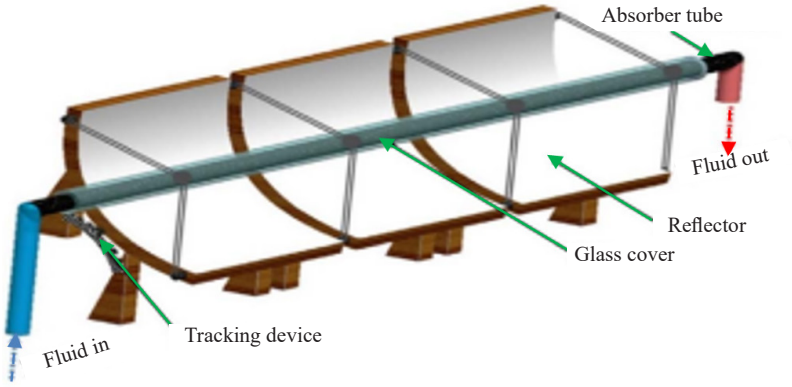

Figure 1. Schematic diagram of a PTSC

Chemically reactive hybrid nanofluid flow across a Riga plate with nonlinear thermal radiation and a changing heat source/sink was investigated by Algehyne et al. [5]. This article aims to explore the flow of a hybrid nanofluid across a three-dimensional stretching surface, where the fluid is affected by chemical reactions, thermal radiation, and a changing thermal source/sink. An increase in the ratio parameter was found to cause the hybrid nanofluid velocity to decrease along the primary direction while increasing along the secondary direction.

The study of hybrid nanofluid Stagnation point flow across a stretched surface with melting heat transfer was investigated by Jawad et al. [6]. This study looked at the behavior of a hybrid nanofluid and stagnation point flow toward a stretched surface in addition to melting heat transfer, second-order slip, electric field, and magnetic field effects. Alumina and copper hybrid nanoparticles are compared with water-based base fluids. The research reveals that the velocity profile decreases as the magnetic field grows as well as the slip parameter and electric field increase. Using fuzzy volume fraction, Verma et al. [7] investigated the impact of heat transfer on hybrid nanofluid flow in converging/diverging channels. This work uses hybrid nanoparticles, Cu and Cu-Al_2O_3, to investigate the magnetohydrodynamic (MHD) Jeffery-Hamel nanofluid flow between two stiff non-parallel plane walls with heat transmission. In this case, the MHD nanofluid flow issue is expanded to include fuzzy volume fraction and heat transfer using a variety of nanoparticles to address the impact of hybrid nanoparticle thermal profiles on fuzzy velocity profiles. The Cu/H_2O and Cu-Al_2O_3/H_2O nanofluid velocity profiles were found to be the same in both channels. Nonetheless, in both channels, the temperature profile of the hybrid nanofluid Cu-Al_2O_3/H_2O is greater than that of the Cu/H_2O nanofluid. CuO, Al_2O_3, and Ag nanomaterials on unsteady stagnation point flow of Oldroyd-B-power-law nanofluid with viscous dissipation were investigated by Bai et al. [8]. This research examines the viscoelasticity and shear thinning properties of an Oldroyd-B-power-law nanofluid with an unstable stagnation-point flow. The heat transfer process's thermal relaxation and thermal retardation were explained using the modified Cattaneo-Christov heat flow model. The result shows that given Deborah's numbers for relaxation and retardation times, the velocity retains an opposing trend. Ag nanoparticles also have the highest capacity to enhance heat transfer of any of the three nanofluids, which can offer a theoretical foundation for industrial processing.

The unsteady hybrid nanofluid flow involving CuO and Al_2O_3/$C_2H_6O_2$ achieved by an oscillating disk immersed in the porous media is highlighted in the study [9] of the hybrid nanofluid flow induced by an oscillating disk, which took

into account the shape factor of nanoparticles and the surface catalyzed reaction. The study also considered the surface-catalyzed reaction to minimize the reaction time in a study of the homogeneous and heterogeneous reactions, where the oscillation and surface-catalyzed chemical reactions have opposite impacts on the concentration profile. The analysis also includes a comparison of the proposed model with a published result in a limiting case.

The increase of heat and mass transfer of MHD hybrid nanofluid flow in the presence of activation energy was investigated by Shanmugapriya et al. [10]. In this investigation, two different kinds of hybrid nanoparticles-single-walled CNTs (SWCNTs) and multi-walled CNTs (MWCNTs)-are suspended in water, which is used as a typical fluid. To further investigate the fine point of hybrid nanofluid flow, the effects of heat radiation, activation energy, and a magnetic field were included. In comparison to previous hybrid nanofluids, the results show that this one is completely sufficient for both heating and cooling. Additionally, the hybrid nanofluid's nanoparticle transfer rate increases as the activation energy value rises. The work conducted by Khan et al. [11] examines the effects of non-fourier heat flux and transitive magnetic field on heat transfer in time-dependent Blasius-Rayleigh-Stoke flow conveying hybrid nano-fluid. The investigation revealed that while the hybrid nanoparticle increases the temperature distribution, it decreases the velocity field.

The influence of the Cattaneo-Christov heat flux on the hybrid nano-fluid flow of Al_2O_3-Cu/H_2O-$(CH_2OH)_2$ between two stretchable spinning disks was elucidated by Shaw [12]. The outcome demonstrates that, in comparison to regular nanofluid, hybrid nanofluid has a greater impact on increasing nusselt number and temperature profile. A comparative investigation of heat transfer and friction drag in the flow of several hybrid nanofluids impacted by nonlinear radiation and an aligned magnetic field is conducted by Khan et al. [13]. The article's main goal is to go over how several hybrid nanofluids and a basic nanofluid affect heat transmission and friction drag on a stretched surface. The findings of this contemporary study indicate that when compared to other hybrid nanofluids like Cu-Al_2O_3/H_2O, Cu-Al_2O_3/$C_2H_6O_2$, and a basic nanofluid like Al_2O_3/H_2O, the hybrid nanofluid Cu-Al_2O_3/H_2O-$C_2H_6O_2$ is very efficient in cooling and heating. These results led to the conclusion that a higher rate of heat transfer and a reduction in friction drag is obtained when numerous particles are suspended in a mixture of two or more base fluids. Cu-Al_2O_3-H_2O hybrid nanofluid flow with melting heat transfer, irreversibility analysis, and nonlinear thermal radiation was studied by Mabood et al. [14]. The outcome shows that when the volume percentage of the nanoparticles increases, the fluid's velocity decreases.

TiO_2-Cu/H_2O hybrid nanofluid with slip conditions in MHD peristaltic flow of Jeffrey material was investigated by Gireesha et al. [15]. A temperature rise was inferred from the intensification of the Brinkman, Grashof, Hartman, thermal slip, and heat production parameters. Gireesha et al. [16] investigated the flow of a hybrid nano-fluid across a permeable longitudinal moving fin in conjunction with natural convection and heat radiation. The outcome demonstrates that natural convection and heat radiation have a major impact on fin cooling. The research papers [17]-[30] that follow are more helpful in comprehending the idea of the hybrid nanoparticles approach. Researchers [31]-[40] looked at how nanofluids may improve heat transfer in various kinds of solar energy systems. Some benefits that nanofluids offer to solar energy systems are as follows:

• The thermal conductivity of a base fluid increases significantly with the addition of nanoparticles.

• The required heat transfer rate, energy consumption, and overall cost of solar energy systems are all reduced by using nanofluids.

• Nanofluids are regarded as excellent absorbing media because of their high absorption coefficients and remarkable stability at high temperatures.

• Due to their reduced surface area need for heat transmission, solar energy systems utilizing nanofluids have shown to be more cost-effective.

The present study seeks to examine the heat and mass transfer of Casson hybrid nano-fluid flow over an inclined surface using the Blasius Rayleigh-Stokes variable. The non-Newtonian Casson nanofluid flow over a stretched sheet through a porous medium has gotten a lot of interest in the last several decades because of its diverse industrial and biological uses. However, relatively no studies have been conducted on Casson hybrid nano-fluid flow over an inclined surface using the Blasius Rayleigh-stokes variable. Copper particles (Cu) and zirconium dioxide (ZrO_2) nanoparticles have been added as nanoparticles suspended in ethylene glycol (EG), the standard fluid, to further enhance the base fluid's capacity to transport heat. Applications for hybrid nanofluids include solar aircraft systems, car radiators, electronic cooling systems, lubrication, biomedicine, and solar heating, among other heat transfer processes. The aforementioned research gap and the significant applications of hybrid nanofluids serve as driving forces for the authors'

work on the project.

2. Model formulations

Considering a two-dimensional time-dependent boundary layer Casson Hybrid Nano-fluid flow over an Inclined Surface using Blasius Rayleigh-Stokes Variable. The nanofluid model that was introduced by Tiwari and Das [41] is taken into consideration for analyzing the constitutive flow of copper, zirconium dioxide, and ethylene glycol at the contact volume fraction for solar aircraft. The flow configuration of the problem is schematically shown in Figure 2. The equations that control the isotropic as well as incompressible Casson flow are as follows:

$$\tau_{ij} = \begin{cases} 2\left(\mu_B + \dfrac{P_y}{\sqrt{2\pi}}\right)e_{ij}, & \pi > \pi_c \\ 2\left(\mu_B + \dfrac{P_y}{\sqrt{2\pi_c}}\right)e_{ij}, & \pi < \pi_c \end{cases} \tag{1}$$

Where, τ_{ij}, μ_B, P_y, $\pi = e_{ij}e_{ij}$, $e_{ij} = (i, j)th$, π_c are respectively the Stress tensor, the dynamic viscosity of the Non-Newtonian fluid, the Fluid yield stress of the liquid, the product of the rate of strain tensor with tensor, the component of the deformation rate, and the critical value of the product based on the non-Newtonian model. The aligned magnetic effect is enforced on the fluid flow with an acute angle α, and is illustrated as: $B = \dfrac{B_0}{\sqrt{(\cos\alpha)\upsilon t + (\sin\alpha)\upsilon x / U_W}}$, where, $B_0 \neq 0$.

The leading governing equations for the flow in the present problem are [13]:

$$\partial_x(u) + \partial_y(v) = 0, \tag{2}$$

$$\rho_{hnf}\left[u\partial_x(u) + v\partial_y(u) + \partial_t(u)\right] = \mu_{hnf}\partial_{yy}(u)\left(1 + \frac{1}{\beta}\right)$$

$$-\sigma_{hnf}{}^4 B_0^2 \sin^2\Gamma_B(u)$$

$$-\frac{u_{hnf}}{(KP)_0}\left(1 + \frac{1}{\beta}\right)(u) - \frac{b^*}{(KP)_0}(u^2), \tag{3}$$

$$(\rho C_p)_{hnf}\left[u\partial_x(T) + v\partial_y(T) + \partial_t(T)\right] = k_{hnf}\partial_{yy}(T) + \mu_{hnf}(\partial_y(u))^2\left(1 + \frac{1}{\beta}\right)$$

$$+\frac{16\sigma^* T_\infty^3}{3k^*}\partial_{yy}(T) + \sigma_{hnf}B_0^2 \sin^2\Gamma_B(u^2)$$

$$+\frac{\mu_{hnf}}{(KP)_0}\left(1 + \frac{1}{\beta}\right)(u^2) + \frac{b^*}{(KP)_0}(u^3), \tag{4}$$

Where the velocity components along x and y are represented as u and v, B_0 denotes magnetic field strength, and U_∞

is the free stream velocity of the fluid. The equations are considered subject to the following boundary conditions [13]:

$$\text{at } y = 0 : u = 0,\ v = 0,\ T = T_w,$$

$$\text{at } y \to \infty : u \to u_\infty,\ T \to T_\infty. \tag{5}$$

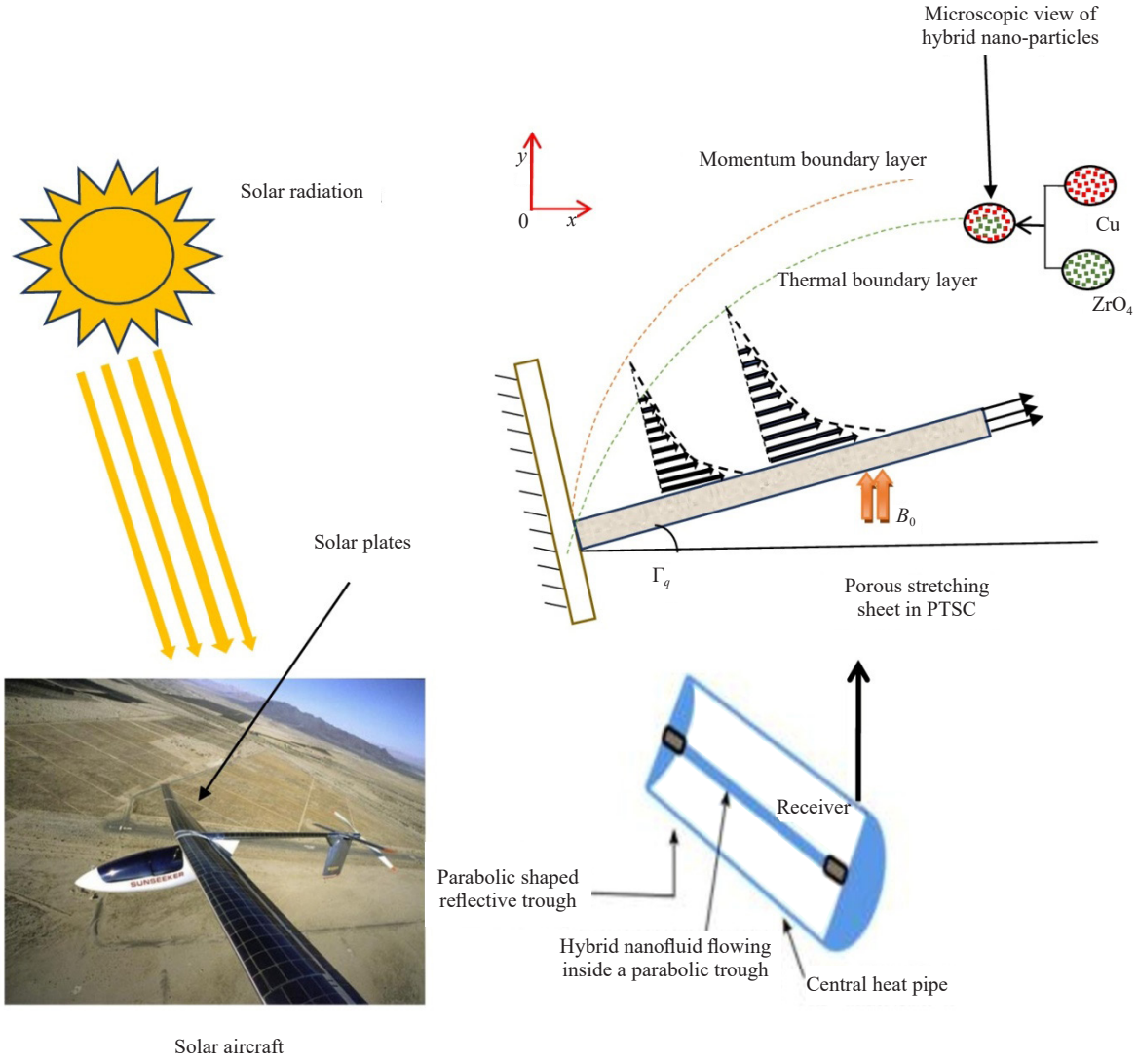

Figure 2. The physical geometry flow

2.1 *Thermophysical possessions of hybrid nanofluid [21]*

$$\mu_{hnf} = \mu_f (1-\phi_1)^{-2.5} (1-\phi_2)^{-2.5},$$

$$\rho_{hnf} = \rho_f \left\{ (1-\phi_1) \left[(1-\phi_2) + \phi_2 \frac{\rho_2}{\rho_f} \right] + \phi_1 \frac{\rho_1}{\rho_f} \right\},$$

$$(\rho C_p)_{hnf} = (\rho C_p)_f \left\{ (1-\phi_1) \left[(1-\phi_2) + \phi_2 \frac{(\rho C_p)_{s2}}{(\rho C_p)_f} \right] + \phi_1 \frac{(\rho C_p)_{s1}}{(\rho C_p)_f} \right\},$$

$$\frac{\sigma_{(hnf)^2}}{\sigma_{nf}} = \left(\frac{(1+2\phi_2)\sigma_2 + (1-2\phi_2)\sigma_{nf}}{(1-\phi_2)\sigma_2 + (1+\phi_2)\sigma_{nf}} \right),$$

$$\frac{\sigma_{nf}}{\sigma_f} = \left(\frac{(1+2\phi_1)\sigma_1 + (1-2\phi_1)\sigma_f}{(1-\phi_1)\sigma_1 + (1+\phi_1)\sigma_f} \right),$$

$$\frac{k_{(hnf)^2}}{k_{nf}} = \left(\frac{k_2 + 2k_{nf} - 2\phi_2(k_{nf} - k_2)}{k_2 + 2k_{nf} + \phi_2(k_{nf} - k_2)} \right),$$

$$\frac{k_{nf}}{k_f} = \left(\frac{k_1 + 2k_f - 2\phi_1(k_f - k_1)}{k_1 + 2k_f + \phi_1(k_f - k_1)} \right). \tag{6}$$

In the above equations, μ_{hnf}, ρ_{hnf}, $(\rho C_p)_{hnf}$, and k_{hnf} indicate the viscosity, density, Specific heat, and thermal conductivity, respectively. Also, ϕ is the nanoparticle fractional volume, and the number of powers each property carries indicates the number of nanoparticles.

2.2 *Nanoparticles (NPs) and base fluid (BF) features*

The Physical features of Ethylene glycol (EG), Copper (Cu), and Zirconium dioxide (ZrO_2) are revealed in Table 1.

Table 1. The physical characteristics of the base fluid and hybrid nanofluid [28]

Physical property	EG	Cu	ZrO_2
$\rho/(kg \cdot m^{-3})$	1,110	8,933	5,680
$k/(W \cdot mK^{-1})$	0.253	401.00	1.7
$C_p/(J \cdot kgK^{-1})$	22,000	385.0	502
$\sigma/(S \cdot m^{-1})$	5.5×10^{-6}	5.96×10^{7}	3×10^{-5}

2.3 *Similarity rules*

The following transformations are generated in transforming the modeled equations [13]:

$$\theta(\eta) = \frac{T - T_\infty}{T_w - T_\infty},$$

$$\eta = \frac{y}{\sqrt{(\cos\alpha)vt + (\sin\alpha)\frac{vx}{U_\infty}}},$$

$$\psi(x,y,t) = U_\infty \sqrt{(\cos\alpha)vt + (\sin\alpha)\frac{vx}{U_\infty}} f(\eta). \tag{7}$$

where

$$u = \partial_y(\psi),\ v = -\partial_x(\psi).$$

2.4 *Transformed problems*

The momentum and thermal characteristics of the hybrid nanofluid are plugged by the transformation.

$$\left(1+\frac{1}{\beta}\right) f''' + \frac{\phi_A\phi_B\eta(\cos\alpha)}{2} f'' + \frac{\phi_A\phi_B(\sin\alpha)}{2} ff'' - \phi_A\phi_C M \times \sin^2\Gamma_B f'$$

$$-\left(1+\frac{1}{\beta}\right) Ppf' - \phi_A\phi_B Fs(f')^2 = 0 \tag{8}$$

$$\theta''\left(1+\frac{1}{\phi_D}PrNd\right) + Pr\frac{\phi_E}{2\phi_D}\eta(\cos\alpha)\theta' + Pr\frac{\phi_E}{2\phi_D}(\sin\alpha) f\theta'$$

$$+\left(1+\frac{1}{\beta}\right)\frac{PrEc}{\phi_A\phi_D}(f'')^2 + EcMPr\frac{\phi_C}{\phi_D}\times\sin^2\Gamma_B(f')^2$$

$$+\left(1+\frac{1}{\beta}\right)\frac{PrEc}{\phi_A\phi_D}(f'')^2 + \frac{PrEcFs}{\phi_D}(f')^3 = 0 \tag{9}$$

Subjected to

$$f(0) = 0,\ f'(0) = 0,\ \theta(0) = 1,$$

$$f'(\eta) \to 1,\ \theta(\eta) \to 0,$$

$$\text{as } \eta \to \infty, \tag{10}$$

Where

$$\phi_A = (1-\phi_1)^{2.5}(1-\phi_2)^{2.5},$$

$$\phi_B = (1-\phi_1)\left[(1-\phi_2)+\phi_2\frac{\rho_2}{\rho_f}\right]+\phi_1\frac{\rho_1}{\rho_f},$$

$$\phi_C = \left(\frac{(1+2\phi_1)\sigma_1+(1-2\phi_1)\sigma_f}{(1-\phi_1)\sigma_1+(1+\sigma_1)\sigma_f}\right)\left(\frac{(1+2\phi_2)\sigma_2+(1-2\phi_2)\sigma_{nf}}{(1-\phi_2)\sigma_2+(1+\phi_2)\sigma_{nf}}\right),$$

$$\phi_D = \left(\frac{k_1+2k_f-2\phi_1(k_f-k_1)}{k_1+2k_f+\phi_1(k_f-k_1)}\right)\left(\frac{k_2+2k_{nf}-2\phi_2(k_{nf}-k_2)}{k_2+2k_{nf}+\phi_2(k_{nf}-k_2)}\right),$$

$$\phi_E = (1-\phi_1)\left[(1-\phi_2)+\phi_2\frac{(\rho C_p)_{s2}}{(\rho C_p)_f}\right]+\phi_1\frac{(\rho C_p)_{s1}}{(\rho C_p)_f}.$$

2.5 *Explanation of the entrenched control constraints*

The thermophysical features of hybrid nanofluid flow and the symbols utilized in the current investigation are detailed in Table 2.

Table 2. below lists the governing equation's control parameters and range values

Parameters	Formulas	Symbols
Porosity parameter	$Pp = \frac{c}{(KP)_0}$	Pp
Eckert number	$Ec = \frac{U_\infty^2}{(C_p)_f(T_w - T_\infty)}$	Ec
Forchheimer parameter	$Fs = \frac{b^* U_\infty c}{\upsilon_f (KP)_0}$	Fs
Radiation parameter	$Nd = \frac{16}{3}\frac{\sigma^* T_\infty^3}{k^* k_f}$	Nd
Magnetic parameter	$M = \frac{\sigma_f \beta_0^2}{\mu_f}$	M
Prandtl number	$Pr = \frac{(\rho C_p)_f \upsilon_f}{k_f}$	Pr

2.6 *Physical quantities*

The drag-force (C_f) and Nusselt number (Nu_x) are the other two physical Quantities requirements for the practicality and utility of engineering, and they are defined as follows:

$$Re_x^{1/2} C_f = \frac{1}{\phi_A \phi_B \sqrt{(\cos\alpha) vt + (\sin\alpha)\frac{vx}{U_\infty}}} \left(1 + \frac{1}{\beta}\right) f''(0)$$

and

$$Re_x^{1/2} Nu_x = -\frac{\phi_D (1 + Nr)}{\sqrt{(\cos\alpha) vt + (\sin\alpha)\frac{vx}{U_\infty}}} \theta'(0) \tag{11}$$

where local Reynolds number $Re_x = \frac{U_\infty x}{v_f}$.

3. GWRM application

A numerical technique called the Galerkin-weighted residual approach uses weighted residuals to solve partial differential equations (PDEs). This numerical scheme proves to be quite helpful in solving boundary conditions (BC) issues that might be difficult for another numerical scheme to solve. The following are the crucial phases in the GWRM: The first thing to do is to examine equations (8) and (9), and the numerical result of equations (8)-(9) is simulated in Step 2 by the Galerkin-weighted residual approach using a specific trail function, which may be investigated as follows:

$$\tilde{f}(\eta) = a^*_0 + a^*_1 e^{-\frac{\eta}{3}} + a^*_2 e^{-\frac{2\eta}{3}} + a^*_3 e^{-2\eta} + \ldots + a^*_n e^{-\frac{n\eta}{3}}$$

$$= \sum_{j=0}^{n} a^*_j e^{-\frac{j\eta}{3}}, \tag{12}$$

$$\tilde{\theta}(\eta) = b^*_0 + b^*_1 e^{-\frac{\eta}{3}} + b^*_2 e^{-\frac{2\eta}{3}} + b^*_3 e^{-2\eta} + \ldots + b^*_n e^{-\frac{n\eta}{3}}$$

$$= \sum_{j=0}^{n} b^*_j e^{-\frac{j\eta}{3}}, \tag{13}$$

Utilizing the reduced trial solutions and the step one procedure, residual vectors for temperature and velocity are created in the fourth step.

$$\left(\frac{d}{d\eta}\sum_{j=0}^{n} a^*_j e^{-\frac{j\eta}{3}}\right)_{\eta=0} = 0,$$

$$\left(\sum_{j=0}^{n} a^*_j e^{-\frac{j\eta}{3}}\right)_{\eta=0} = 0,$$

$$\left(\sum_{j=0}^{n} b^{*}{}_{j} e^{-\frac{j\eta}{3}} - 1\right)_{\eta=0} = 0. \tag{14}$$

Step three of the process is using the GWRM trial solutions to make sure the boundary conditions of (10) and the BCs for the problem are met. These are:

$$R_f = \left(1+\frac{1}{\beta}\right)\tilde{f}''' + \frac{\phi_A\phi_B\eta(\cos\alpha)}{2}\tilde{f}'' + \frac{\phi_A\phi_B(\sin\alpha)}{2}\tilde{f}\tilde{f}''$$

$$-\phi_A\phi_C M \times \sin^2\Gamma_B\tilde{f}' - \left(1+\frac{1}{\beta}\right)Pp\tilde{f}' - \phi_A\phi_B Fs(\tilde{f}')^2 \cong 0, \tag{15}$$

$$R_\theta = \tilde{\theta}''\left(1+\frac{1}{\phi_D}PrNr\right) + Pr\frac{\phi_E}{2\phi_D}\eta(\cos\alpha)\tilde{\theta}' + Pr\frac{\phi_E}{2\phi_D}(\sin\alpha)\tilde{f}\tilde{\theta}'$$

$$+\left(1+\frac{1}{\beta}\right)\frac{PrEc}{\phi_A\phi_D}(\tilde{f}'')^2 + EcMPr\frac{\phi_C}{\phi_D}\times\sin^2\Gamma_B(\tilde{f}')^2$$

$$+\left(1+\frac{1}{\beta}\right)\frac{PrEc}{\phi_A\phi_D}(\tilde{f}'')^2 + \frac{PrEcFs}{\phi_D}(\tilde{f}')^3 \cong 0. \tag{16}$$

Step 5: The residual has to be zero over the following domain in order to investigate the constants:

$$\int_0^\infty R_f e^{-\frac{j\eta}{3}} d\eta \approx \sum_{k=1}^{j}\left[A_k\left(e^\eta R_f e^{-\frac{j\eta}{3}}\right)_{\eta=x_k}\right] = 0,$$

$$\int_0^\infty R_\theta e^{-\frac{j\eta}{3}} d\eta \approx \sum_{k=1}^{j}\left[A_k\left(e^\eta R_\theta e^{-\frac{j\eta}{4}}\right)_{\eta=x_k}\right] = 0,$$

For $j = 0, 1, 2, ..., N-2,\ l = 0, 12, ..., N-2$ to zero.

Where A_k is described as:

$$A_k = \frac{1}{L_j'(x_k)}\int_0^\infty \frac{L_j(x)e^{-x}}{x-x_k}dx = \frac{(j!)^2}{x_k\left(L_j'(x_k)\right)^2},\ L_j = e^x\frac{d^j}{dx^j}(e^{-x}x^j)$$

To minimize the residual errors, the weight functions $R_f e^{-\frac{j\eta}{4}}$, $R_\theta e^{-\frac{j\eta}{4}}$, and residues product were integrated. Figure 3 displays the flow chart of the GWRM scheme.

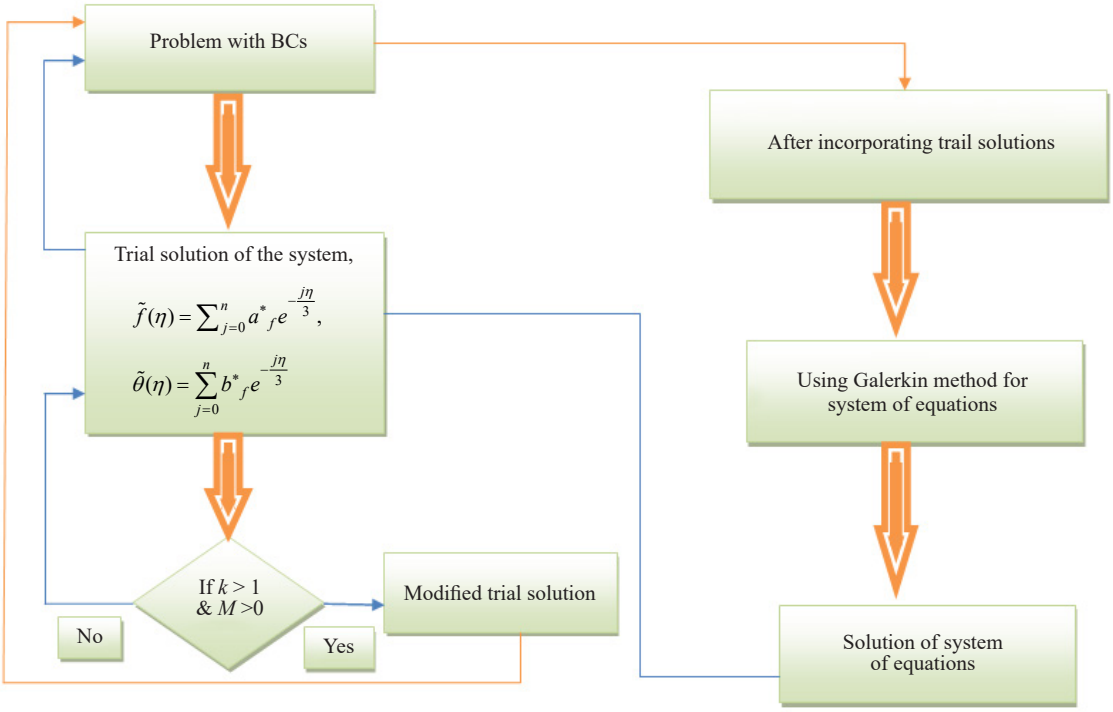

Figure 3. The GWRM flow chart

Table 3. Comparison table for values of Pr obtained for $\varphi_1 = \varphi_2 = Q = Q_1 = Rd = M = \alpha = A_1 = A_2 = Ec = 0$, $Re = 1$

Pr	$-\theta'(0)$ [23]	$-\theta'(0)$ [17]	$-\theta'(0)$ [13]	Present work
0.7	0.292	0.292683	0.29268256	0.292455989874124
0.8	0.307	0.306918	0.30691734	0.305031590809784
1.0	0.332	0.332059	0.33205865	0.328462119365859
5.0	0.585	0.576696	0.57668534	0.576300253464666
6.2 (water)	-	0.620077	0.62007632	0.620230799295692
10	0.730	0.728155	0.72815432	0.729401187629374
21 (Kerosene)	-	0.933538	0.93353719	0.936285109611171

4. Results and discussion

Analysis of non-newtonian Casson hybrid nanofluid flow using Rayleigh Stokes variable with an inclined magnetic field using the GWRM was considered in this paper. ZrO_2 and Cu are the two nanoparticles examined in this research with the mixture of EG as the base fluid. A graphical analysis and explanation of the key parameters' effects on the temperature and velocity profiles for Cu-ZrO_2/EG hybrid nanofluid, and Cu/EG nanofluid are shown in this section. On the graph, the Cu/EG nanofluid is represented by solid lines, while the Cu-ZrO_2/EG hybrid nanofluid is shown by dashed lines. Numerical computations were tabulated and also represented graphically. The physical parameters considered in

this work are stated below and their ranges are given as follows: magnetic parameter $M = 0.2$ ($M = 0.2, 0.4, 0.6, 0.8$), Casson parameter $\beta = 0.5$ ($\beta = 0.2, 0.4, 0.6, 0.8$), Forchheimer parameter $Fs = 0.1$ ($Fs = 2.0, 4.0, 6.0, 8.0$), Leading-edge accretion/ablation parameter $\alpha = \pi/3$ ($\alpha = 0, \pi/3, \pi/2, \pi$), magnetic parameter $\phi_1, \phi_2 = 0.18$ ($\phi = 0.2, 0.4, 0.6, 0.8$), Eckert number $Ec = 0.3$ ($Ec = 2.0, 4.0, 6.0, 8.0$), and thermal radiation $Nd = 0.3$ ($Nd = 2.0, 4.0, 6.0, 8.0$). Comparative analysis was carried out on the present work with some related studies [1]-[4] considering the effect of Nusselt number (Nu_x) on the flow, which is displayed in Table 3, and Table 4 also shows a comparison result for different works [1]-[4] and the present work for various values of Leading edge accretion/ablation parameter.

Table 4. Comparison table for values of α obtained for $\varphi_1 = \varphi_2 = Q = Q_1 = Rd = M = \alpha = A_1 = A_2 = Ec = 0$, $Re = 1$

Accretion rate	α	$f''(0)$ [17]	$f''(0)$ [13]	Present work
Rayleigh-Stokes	0	0.564191	0.56419547	0.5644
(7.596) U_∞	$\pi/24$	0.575018	0.57501546	0.5751
(3.732) U_∞	$\pi/12$	0.580731	0.58073245	0.5808
(1.732) U_∞	$\pi/6$	0.577004	0.57700381	0.5770
U_∞	$\pi/4$	0.552877	0.55287544	0.5529
(0.577) U_∞	$\pi/3$	0.507220	0.50722178	0.5073
(0.268) U_∞	$5\pi/12$	0.436866	0.43686289	0.4374
(0.132) U_∞	$11\pi/24$	0.390000	0.39000000	0.3914
Blasius	$\pi/2$	0.332059	0.33205356	0.3361

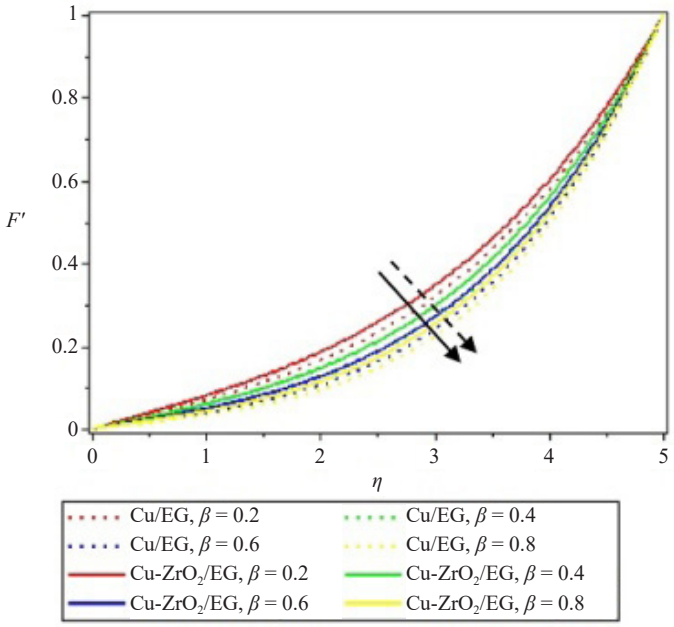

Figure 4. Effect of β on $f'(\eta)$

4.1 *Influence of various physical parameters on the velocity profile for Copper-Zirconium dioxide-ethylene glycol (Cu-ZrO_2/EG) hybrid nanofluid and Copper-ethylene glycol (Cu/EG) nanofluid*

Figure 4 shows the influence of the Casson parameter (β) on the velocity profile of the fluid. It was observed that increasing the Casson parameter reduces the fluid velocity. Physically, increasing the Casson parameter causes an increase in the fluid's dynamic viscosity which reduces fluid motion and results in a decrease in the velocity profile. Therefore, the Casson parameter reduces the yield stress and suppresses the velocity flow. However, the plastic-dynamic viscosity fluid was utilized as a Casson rheological fluid with a strong reaction to yield stress. Because of the increase in the dynamic viscosity of the fluid, there will be an increase in resistance of the fluid velocity. Based on this finding, it was also observed that the velocity profile of Cu/EG nanofluid is higher than that of Cu-ZrO_2/EG hybrid nanofluid; this is because the more particles added the lower the velocity of the medium.

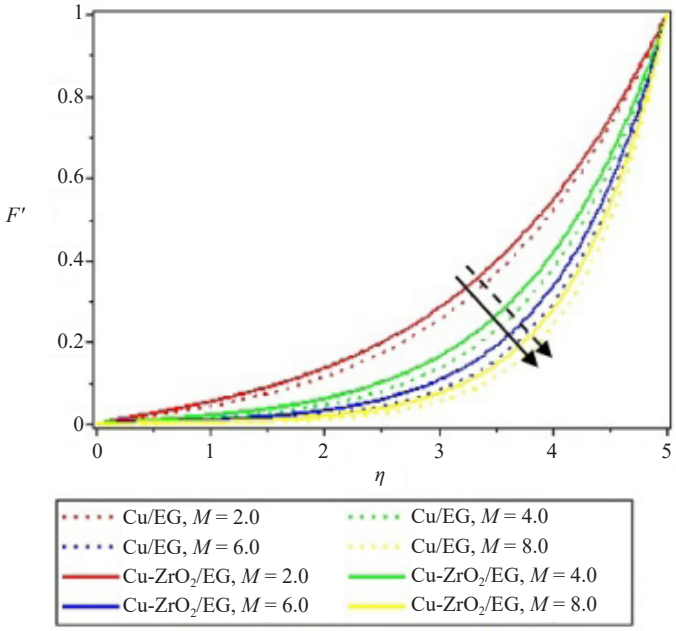

Figure 5. Effect of M on $f'(\eta)$

The influence of the magnetic parameter (M) on the velocity profile of the fluid is depicted in Figure 5. It was discovered that increasing magnetic parameters causes the fluid motion to decrease. Moreover, the magnetic field induces the Lorentz force against the fluid flow. Subsequently, as the drag force intensity, it generates more resistance to transport phenomena by decreasing the fluid velocity. Hence, the magnetic field decreases the thickness of the boundary layer, while the fluid speed of the hybrid nanofluid movement is cooling down the transverse magnetic field in the boundary layer. It was also shown that the velocity distribution rate of Cu/EG nanofluid is higher than that of Cu-ZrO_2/EG hybrid nanofluid. Zirconium dioxide is a white powder that dissolves easily in EG but adds more shear stress to the velocity of the medium.

One of the efficient techniques that might have a big impact on the key elements of this present study, such as fluidity and thermal energy, is the porous constraint. An increase in the Forchheimer parameter value results in a decrease in velocity. The data in Figure 6 indicates that a reduction in the fluid velocity passing through a porous material corresponds with an increase in the permeability of the porous medium. This causes the motion to slow down and creates resistance near the wall surface. A significant increase in the number of flowing pores is indicated by increased porosity. The thickness of the velocity boundary layer increases, so the velocity reduces with an increase in

the porosity parameter, which is due to the fact that the effect of the porous medium that opposes the flow also increases and leads to enhanced deceleration of the flow. It was observed that the velocity profile of Cu/EG nanofluid is higher than that of Cu-ZrO_2/EG hybrid nanofluid.

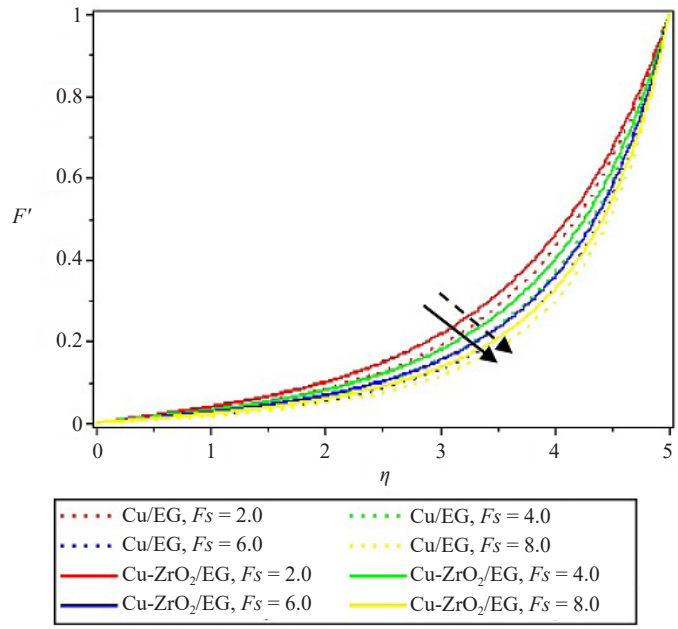

Figure 6. Effect of Fs on $f'(\eta)$

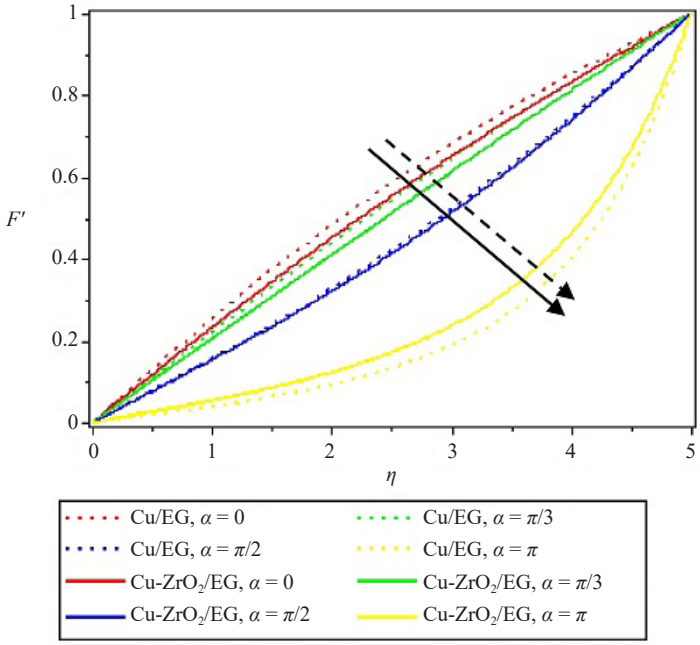

Figure 7. Effect of α on $f'(\eta)$

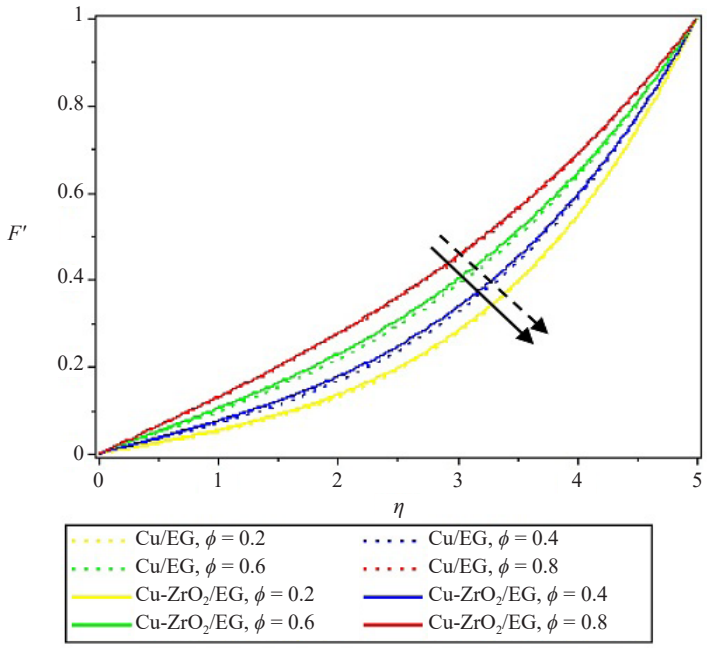

Figure 8. Effect of ϕ on $\theta(\eta)$

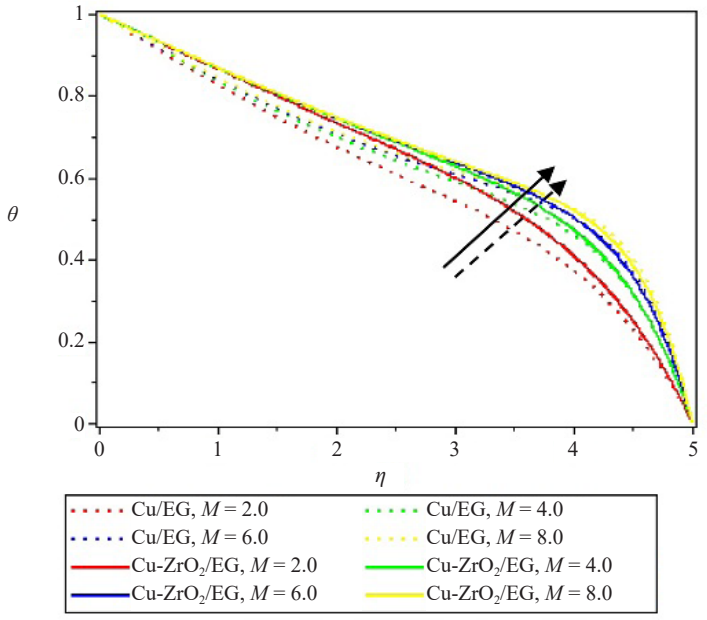

Figure 9. Effect of M on $\theta(\eta)$

The velocity profile carrying Cu/EG nanofluid, and Cu-ZrO_2/EG hybrid nanofluid, varies for different values of the leading edge accretion/ablation parameter (α), as shown in Figure 7. Due to the highest values of (α) the momentum circumferential layer's compactness and velocity profile are slowing down. Additionally, the graph shows that Cu/EG nanofluid has a greater velocity profile than Cu-ZrO_2/EG hybrid nanofluid. Figure 8 illustrates the influence of volume fraction parameters on the velocity distribution for the Cu-ZrO_2/EG hybrid nanofluid, and Cu/EG nanofluid.

The fluid flow's velocity decreases as the Cu-ZrO_2/EG hybrid nanofluid increases. As the (ϕ) parameter increases, the fluid flow's velocity decreases. The hydrodynamic boundary layer's structure intensifies with increasing nanomolecule concentrations. With an increasing (υ) parameter, the Cu-ZrO_2/EG HNF has a higher fluid flow than the Cu/EG NF single nanofluid.

4.2 *Influence of various physical parameters on the temperature profile for Copper-Zirconiumdioxide-ethylene glycol (Cu-ZrO_2/EG) hybrid nanofluid and Copper-ethylene glycol Cu/EG) nanofluid*

It appears as if Cu-ZrO_2/EG is marginally better than Cu/EG in the same place because the presence of the hybrid nanoparticle Cu-ZrO_2/EG in the base fluid hinders the magnetic field's ability to affect the fluid. As a result, there is less Cu/EG nanofluid than Cu-ZrO_2/EG hybrid nanofluid. A rise in the magnetic field term (M) strength has a significant impact on the thermal field. The temperature profile is strongly positively impacted by the increasing (M) intensity (2.0, 4.0, 6.0, and 8.0) (see Figure 9). It is commonly known that higher values of M are associated with a greater Lorentz force, which causes the fluid's velocity to slow down. Because of the additional heat generated by this drag on motion, the temperature field is increased. Because of its narrower thermal barrier structure than the Cu/EG nanofluid, the Cu-ZrO_2/EG hybrid nanoparticle exhibits a lower surface temperature and higher heat transfer as the magnetic field parameter increases.

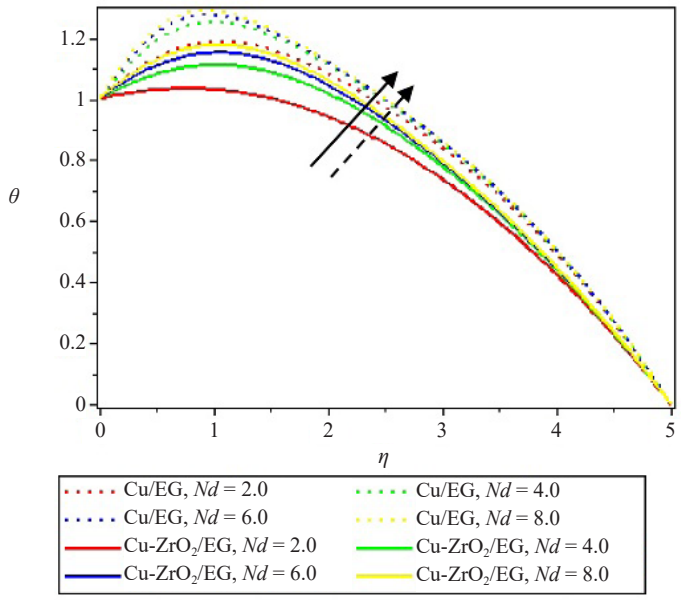

Figure 10. Effect of Nd on $\theta(\eta)$

The temperature of the nanofluid improves as a result of more heat being delivered into the system due to an increase in thermal radiation. These claims are supported by Figure 10. Additionally, the temperature of the nanofluid inside the boundary layer rises with an improvement in the radiation parameter (Nd). The quantity of heat that is transported into the fluid increases with increasing parameter (Nd) value, increasing the thickness of the thermal boundary layer. It is important to remember that radiation has a significant effect on the temperature distribution. As seen in Figure 10, the Cu-ZrO_2/EG hybrid nanofluid has a thinner thermal boundary layer than the Cu/EG nanofluid. A higher number for solar radiation suggests that radiation is stronger than convection. This evolution may be described by the supposition that heat radiation is converted to electromagnetic energy. The influence of (Ec) on the temperature

distributions of Cu/EG nanofluids and Cu-ZrO_2/EG hybrid nanofluids is shown in Figure 11. The general consensus is that all of the energy lost in the system as a result of viscous dissipation will eventually be converted to heat. However, the fluid's temperature rose as additional heat was introduced into the system.

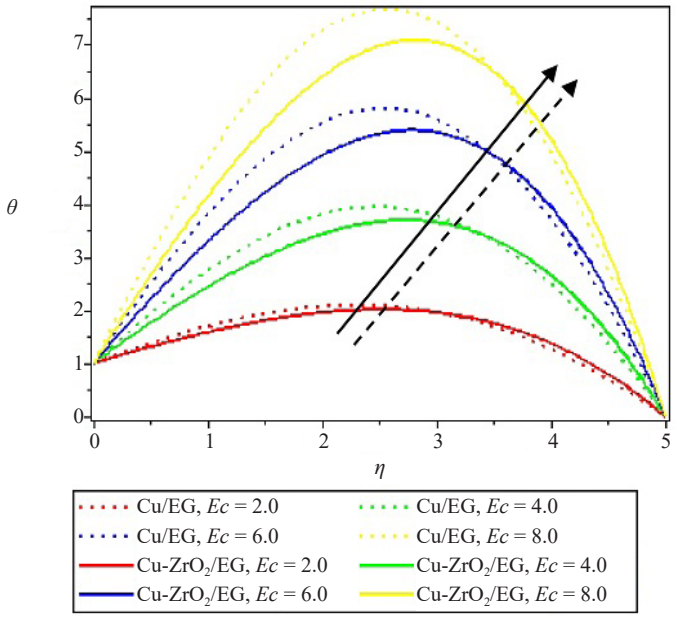

Figure 11. Effect of Ec on $\theta(\eta)$

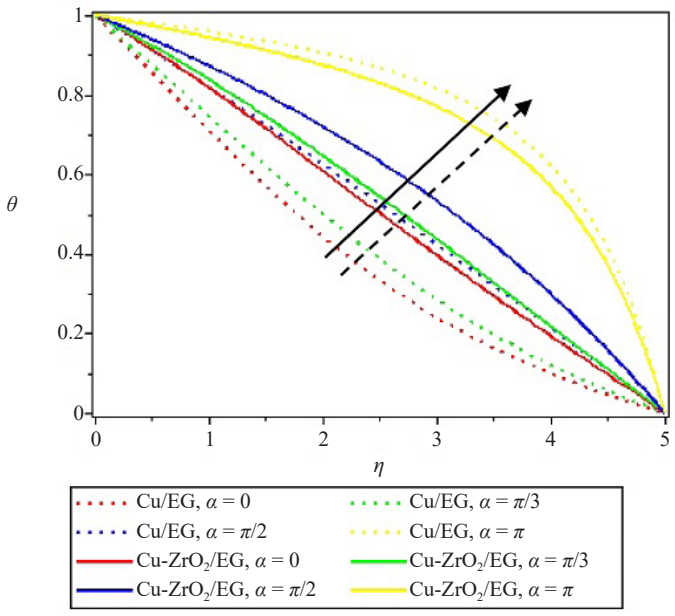

Figure 12. Effect of α on $\theta(\eta)$

Figure 12 illustrates how the temperature profile for the Cu/EG and Cu-ZrO_2/EG hybrid nanofluids changes for various values of the leading edge accretion/ablation parameter (α). The temperature profile is improved and heat rises quickly at the greatest levels of (α). Furthermore, the graph indicates that the temperature profile of Cu/EG nanofluid is higher than that of Cu-ZrO_2/EG hybrid nanofluid.

5. Conclusion

In this study, the Blasius Rayleigh-Stokes variable is used to compute the radiative effect of Casson hybrid nano-fluid flow on an inclined surface. The Casson parameter, magnetic terms, leading-edge accretion/ablation parameter, volume fraction parameters, Eckert number, and thermal radiation are all taken into account in the mathematical model. Graphs and tables that show good relationships with the existing research are produced after the proposed model was analyzed using the GWRM. To the best of the author's knowledge, no research has been published thus far on the topic of Casson hybrid nano-fluid flow over an inclined surface using the Blasius Rayleigh-stokes variable. It was found that the medium's thermal conductivity is positively impacted by the addition of particles smaller than 100 nm to the base fluid and thus the following is a summary of the significant findings that resulted from the current investigation:

- In terms of accuracy and convergence, the Galerkin-weighted residual technique shows a lot of promise.
- The fluidity is delayed by the Casson, Forchheimer, Leading Edge Accretion/Ablation, and Nanoparticle Concentration parameters, for Cu/EG nanofluid and Cu-ZrO_2/EG hybrid nanofluid.
- The efficiency of industrial machinery is supported by the improved rate of heat transfer caused by thermal radiation.
- The magnetic term is positively impacted by the Cu-ZrO_2/EG hybrid nanofluid's thermal distribution.
- The Cu/EG nanofluid that convects produces a higher degree of heat radiation.

In order to provide more direction and support future studies, it is required to include more characteristics in the flow performance at higher values of the thermal conductivity parameter. Second-order slip, activation energy, magneto-slip, and thermal criticality are some of the additional factors that may be considered, but the process of determining these extra factors has to be put into practice soon.

Acknowledgment

The authors applaud the excellent research facilities of Ladoke Akintola University of Technology's Department of Pure and Applied Mathematics.

Data availability statement

All of the information and resources produced during this inquiry are included in this research article. This work has data associated with it in a data repository. [Authors comment: Upon request, any of the data utilized in this work may be obtained from the appropriate author].

Conflict of interests

There are no competing interests declared by the author(s).

References

[1] O. Juszczyk, J. Juszczyk, S. Juszczyk, and J. Takala, "Barriers for renewable energy technologies diffusion: Empirical Evidence from Finland and Poland," *Energies*, vol. 15, no. 2, pp. 527-542, 2022.

[2] A. Kumar, P. Singh, P. Raizada, and C. M. Hussain, "Impact of COVID-19 on greenhouse gases emissions: A critical review," *Science of the Total Environment*, vol. 806, pp. 150349, 2022.
[3] M. D. Mathew, "Nuclear energy: A pathway towards mitigation of global warming," *Progress in Nuclear Energy*, vol. 143, pp. 104080, 2022.
[4] R. K. Singh and P. Chandra, "Parabolic trough solar collector: A review on geometrical interpretation, mathematical model, and thermal performance augmentation," *Engineering Research Express*, vol. 5, pp. 012003, 2023.
[5] E. A. Algehyne, S. A. Lone, Z. Raizah, S. M. Eldin, A. Saeed, and A. M. Galal, "Chemically reactive hybrid nanofluid flow past a Riga plate with nonlinear thermal radiation and a variable heat source/sink," *Frontiers in Materials*, vol. 10, pp. 1132468, 2023.
[6] M. Jawad, Z. Khan, E. Bonyah, and R. Jan, "Analysis of hybrid nanofluid stagnation point flow over a stretching surface with melting heat transfer," *Mathematical Problems in Engineering*, vol. 2022, pp. 9469164, 2022.
[7] L. Verma, R. Meher, Z. Hammouch, and H. M Baskonus, "Effect of heat transfer on hybrid nanofluid flow in converging/diverging channel using fuzzy volume fraction," *Scientific Reports*, vol. 12, no. 1, pp. 20845, 2022.
[8] Y. Bai, H. Fang, and Y. Zhang, "Investigation of CuO, Al_2O_3 and Ag nanomaterials on unsteady stagnation point flow of Oldroyd-B-power-law nanofluid with viscous dissipation," *Pramana*, vol. 96, no. 2, pp. 61, 2022.
[9] M. Ramzan, S. Riasat, S. F. Aljurbua, H. A. S. Ghazwani, and O. Mahmoud, "Hybrid nanofluid flow induced by an oscillating disk considering surface catalyzed reaction and nanoparticles shape factor," *Nanomaterials*, vol. 12, no. 11, pp. 1794, 2022.
[10] M. Shanmugapriya, R. Sundareswaran, and S. P. Kumar, "Heat and mass transfer enhancement of MHD hybrid nanofluid flow in the presence of activation energy," *International Journal of Chemical Engineering*, vol. 2021, pp. 1-12, 2021.
[11] M. R. Khan, M. Li, S. Mao, R. Ali, and S. Khan, "Comparative study on heat transfer and friction drag in the flow of various hybrid nanofluids effected by aligned magnetic field and nonlinear radiation," *Scientific Reports*, vol. 11, no. 1, pp. 3691, 2021.
[12] S. Shaw, "Impact of cattaneo-Christov heat flux On Al_2O_3-Cu/H_2O-$(CH_2OH)_2$ hybrid nanofluid flow between two stretchable rotating disks," in *Energy Systems and Nanotechnology*, D. Tripathi and R. K. Sharma, Eds. Singapore: Springer, 2021, pp 329-368.
[13] U. Khan, A. Zaib, A. Ishak, and S. A. Bakar, "Time-dependent Blasius-Rayleigh-Stokes flow conveying hybrid nanofluid and heat transfer induced by non-Fourier heat flux and transitive magnetic field," *Case Studies in Thermal Engineering*, vol. 26, pp. 101151, 2021.
[14] F. Mabood, T. A. Yusuf, and W. A. Khan, "Cu-Al_2O_3-H_2O hybrid nanofluid flow with melting heat transfer, irreversibility analysis and nonlinear thermal radiation," *Journal of Thermal Analysis and Calorimetry*, vol. 143, no. 2, pp. 973-984, 2021.
[15] B. J. Gireesha, K. Gangadhar, S. P. Manasa, and S. Sindhu, "Entropy generation analysis of electrical magnetohydrodynamic flow of TiO_2-Cu/H_2O hybrid nanofluid with partial slip," *International Journal of Numerical Methods for Heat & Fluid Flow*, vol. 31, no. 6, pp. 1905-1929, 2021.
[16] B. J. Gireesha, G. Sowmya, M. I. Khan, and H. F. Öztop, "Flow of hybrid nanofluid across a permeable longitudinal moving fin along with thermal radiation and natural convection," *Computer Methods and Programs in Biomedicine*, vol. 185, pp. 105166, 2020.
[17] M. R. Ilias, N. S. Ismail, N. H. Ab Raji, N. A. Rawi, and S. Shafie, "Unsteady aligned MHD boundary layer flow and heat transfer of a magnetic nanofluids past an inclined plate," *International Journal of Mechanical Engineering and Robotics Research*, vol. 9, no. 2, pp. 197-206, 2020.
[18] A. M. Obalalu, A. O. Ajala, A. O. Akindele, O. A. Areo, S. D. Ogundiran, K. A. Salaudeen, and S. Alao, "Entropy generation minimization for radiative casson fluid flow through permeable walls and convective heating: A comprehensive numerical investigation," *Defect and Diffusion Forum*, vol. 415, pp. 21-38, 2020.
[19] A. M. Obalalu, A. O. Ajala, A. O. Akindele, O. A. Oladapo, O. O. Akintayo, and O. M. Jimoh, "Computational study of magneto-convective non-Newtonian nanofluid slip flow over a stretching/shrinking sheet embedded in a porous medium," *Computers Mathematics with Applications*, vol. 119, pp. 319-326, 2022.
[20] A. O. Akindele, O. A. Wale, A. M. Obalalu, A. Peter, A. O. Adebayo, and S. Alao, "MHD flow of nano-fluid with non-uniform heat source or sink in the presence of chemical reaction and activation energy," *Journal of Advance Research in Applied Science*, vol. 7, no. 5, pp. 1-15, 2021.
[21] T. Oreyeni, A. O. Akindele, A. M. Obalalu, O. S. Salawu, and K. Ramesh, "Thermal performance of radiative magnetohydrodynamic Oldroyd-B hybrid nanofluid with Cattaneo-Christov heat flux model: Solar-powered ship application," *Numerical Heat Transfer, Part A: Applications*, pp. 1-19, 2023.

[22] O. A. Ajala and A. Peter, "Hydromagnetic flow of micropolar nanofluids with co-effects of thermal radiation and chemical reaction over an inclined permeable stretching surface," *Beni-Suef University Journal of Basic and Applied Sciences*, vol. 12, no. 1, pp. 86, 2023.
[23] A. Bejan, *Convection Heat Transfer*, New Jersey: John Wiley & Sons, 2013.
[24] A. O. Akindele and A. W. Ogunsola, "A study of non-isothermal permeable flow of nano-fluids in a stretchable rotating disk system," *Journal of Mathematical and Computational Science*, vol. 11, no. 2, pp. 1486-1498, 2021.
[25] A. M. Obalalu, O. A. Ajala, A. Abdulraheem, and A. O. Akindele, "The influence of variable electrical conductivity on non-Darcian Casson nanofluid flow with first and second-order slip conditions," *Partial Differential Equations in Applied Mathematics*, vol. 4, no. 1, pp. 100084, 2021.
[26] O. S. Mate, A. M. Obalalu, O. A. Ajala, T. B. Bakare, A. W. Ogunsola, and A. O. Akindele, "Thermal radiation effect on non-newtonian casson fluid through a porous material over a magnetic field with buoyancy," *International Journal of Thermofluid Science and Technology*, vol. 10, no. 1, 2023.
[27] W. Jamshed, K. S. Nisar, R. W. Ibrahim, F. Shahzad, and M. R. Eid, "Thermal expansion optimization in solar aircraft using tangent hyperbolic hybrid nanofluid: A solar thermal application," *Journal of Materials Research and Technology*, vol. 14, pp. 985-1006, 2021.
[28] M. R. Ilias, N. A. Rawi, N. H. A. Raji, and S. Shafie, "Unsteady aligned MHD boundary layer flow and heat transfer of magnetic nanofluid past a vertical flate plate with leading edge accretion," *ARPN Journal of Engineering and Apples Science*, vol. 13, no. 1, pp. 340-351, 2018.
[29] A. W. Ogunsola and A. O. Akindele, "Mixture of Al_2O_3-Cu/H_2O-$(CH_2OH)_2$ MHD hybrid nanofluid flow due to a stretchable rotating disks system under the influence of non-uniform heat source or sink and thermal radiation," *Journal of Mathematical and Computational Science*. vol. 12, no. 1, pp. 1-27, 2022.
[30] T. N. Sindhu, A. B. Çolak, S. A. Lone, A. Shafiq, and T. A. Abushal, "A decreasing failure rate model with a novel approach to enhance the artificial neural network's structure for engineering and disease data analysis," *Tribology International*, vol. 192, pp. 109231, 2024.
[31] A. Shafiq, A. B. Çolak, T. N. Sindhu, S. A. Lone, and T. A. Abushal, "Modeling and survival exploration of breast carcinoma: A statistical, maximum likelihood estimation, and artificial neural network perspective," *Artificial Intelligence in the Life Sciences*, vol. 4, pp. 100082, 2023.
[32] A. Shafiq, A. B. Çolak, and T. N. Sindhu, "Comparative analysis to study the Darcy-Forchheimer Tangent hyperbolic flow towards cylindrical surface using artificial neural network: An application to Parabolic Trough Solar Collector," *Mathematics and Computers in Simulation*, vol. 216, pp. 213-230, 2024.
[33] A. Shafiq, A. B. Çolak, and T. N. Sindhu, "Development of an intelligent computing system using neural networks for modeling bioconvection flow of second-grade nanofluid with gyrotactic microorganisms," *Numerical Heat Transfer, Part B: Fundamentals*, pp. 1-18, 2023.
[34] M. N. Khan, S. Ahmad, Z. Wang, N. A. Ahammad, and M. A. Elkotb, "Bioconvective surface-catalyzed Casson hybrid nanofluid flow analysis by using thermodynamics heat transfer law on a vertical cone," *Tribology International*, vol. 188, pp. 108859, 2023.
[35] S. Nadeem, S. Ahmad, A. Issakhov, and I. M. Alarifi, "MHD stagnation point flow of nanofluid with SWCNT and MWCNT over a stretching surface driven by Arrhenius kinetics," *Applied Mathematics-A Journal of Chinese Universities*, vol. 37, no. 3, pp. 366-382, 2022.
[36] W. F. Xia, S. Ahmad, M. N. Khan, H. Ahmad, A. Rehman, J. Baili, and T. N. Gia, "Heat and mass transfer analysis of nonlinear mixed convective hybrid nanofluid flow with multiple slip boundary conditions," *Case Studies in Thermal Engineering*, vol. 32, pp. 101893, 2022.
[37] F. Wang, J. Zhang, S. Algarni, M. N. Khan, T. Alqahtani, and S. Ahmad, "Numerical simulation of hybrid Casson nanofluid flow by the influence of magnetic dipole and gyrotactic microorganism," *Waves in Random and Complex Media*, pp. 1-16, 2022.
[38] K. G. Kumar, "Impact of magnetic dipole on flow and heat transfer of AA7072-AA7075/water based nanofluid over a stretching sheet using Koo and Kleinstreuer model," *The European Physical Journal Plus*, vol. 137, no. 6, pp. 1-13, 2022.
[39] M. Azam, N. Abbas, K. G. Kumar, and S. Wali, "Transient bioconvection and activation energy impacts on Casson nanofluid with gyrotactic microorganisms and nonlinear radiation," *Waves in Random and Complex Media*, pp. 1-20, 2022.
[40] V. Puneeth, S. Manjunatha, K. G. Kumar, and R. M. Gnaneswara, "Perspective of multiple slips on 3D flow of Al_2O_3-TiO_2-CuO/H_2O ternary nanofluid past an extending surface due to non-linear thermal radiation," *Waves in Random and Complex Media*, pp. 1-19, 2022.

[41] R. J. Tiwari and M. K. Das, “Heat transfer augmentation in a two-sided lid-driven differentially heated square cavity utilizing nanofluids,” *International Journal of Heat and Mass Transfer*, vol. 50, no. 9-10, pp. 2002-2018, 2007.